Principles of magnetic resonance imaging

A.O. Rodríguez
Centro de Inestigación en Imagenología e Instrumentación Médica,
Universidad Autónoma Metropolitana Iztapalapa,
Av. San Rafael Atlixco 186, México, D. F., 09340. México,
Telephone No.: 85 02 45 69, Fax No.: (5255) 5804-4631,
e-mail: arog@xanum.uam.mx

Recibido el 25 de agosto de 2003; aceptado el 8 de diciembre de 2003

The concepts of magnetic resonance imaging are reviewed and its application to medical and biological systems is described. The magnetic resonance phenomenon can be described by both classical and quantum mechanical approaches. Magnetic resonance imaging is based on the techniques of nuclear magnetic resonance. The scanner first aligns the nuclear spins of hydrogen atoms in the patient and starts rotating them in a perfect concert. The nuclei emit maximum-strength electromagnetic waves at the start, but over time the rotating spins get out of synch, simply due to small differences in local magnetic fields. The unsynchronized spins cause the combined electromagnetic signal to decay with time, a phenomenon called relaxation. A slice is selected applying a gradient in a particular direction (*X*, *Y* or *Z*). Magnetic resonance signals are then formed by means of the application of magnetic field gradients along three different directions. Finally, the signals are acquired and Fourier transformed to form a two-dimensional or three-dimensional image. Important parameters determining the image quality such as signal-to-noise ratio, contrast and resolution are discussed too. A review of the most widely utilised imaging techniques is given including ultra-fast sequences.

Keywords: Magnetic resonance imaging; pulse sequences; ultra-fast imaging.

Los conceptos de la imagenología por resonancia magnética son revisados y se describen algunas de sus aplicaciones a sistemas biológicos y médicos. El fenómeno de resonancia magnética puede describirse tanto con un enfoque mecánico cuántico como clásico. El escaner primero alinea los núcleos de los espines de los átomos de hidrógeno que se encuentran dentro del paciente, y luego comienza a rotarlos de acuerdo a un concierto perfecto. Los núcleos emiten ondas electromagnéticas al inicio, pero a medida que transcurre el tiempo los espines pierden la sincronización, debido simplemente a un decaimiento que representa el denominado fenómeno de relajación. Posteriormente se selecciona una rebanada por medio de la aplicación de un gradiente de campo magnético en un dirección particular (*X*, *Y* o *Z*). A las señales de resonancia magnética que se generan se les aplica la transformada de Fourier para formar una imagen bidimensional o tridimensional. También se estudian los parámetros que determinan la calidad de la imagen como el cociente señal a ruido, el contraste y la resolución. Además, se presenta un breve resumen de las secuencias imagenológicas más usadas incluyendo las secuencias ultra rápidas.

Descriptores: Imagenología por resonancia magnética; secuencias de pulsos; imagenología ultra rápida.

PACS: 42.30.Va; 76.60.Lz; 76.60.Pc; 87.57.-s; 87.61.-c; 87.61.Cd; 87.63.-d

1. Introduction

The first successfull nuclear magnetic resonance experiment in condensed matter (as opposed to those using beams of particles in high vacuum) was carried out in the laboratories of Bloch and Purcell about 58 years ago [1-5]. For this work, they shared the Nobel prize in physics in 1952. These experiments layed the foundations of the magnetic resonance imaging (MRI) and spectroscopy (MRS) applied to biomedical sciences. Around 21 years later, two pioneering papers by Lauterbur [6], and Mansfield, and Granell [7], published within a few months of one another, independently proposed to use the NMR to form an image. This imaging modality was named NMRI, however, due to the widespread concern over any phrase containing the word nuclear, the acronym was changed to MRI. This imaging modality is a powerful tool because of its flexibility and sensitivity to a broad range of tissue properties. Its noninvasive nature makes it an highly demanded technique to diagnose a wide variety of diseases.

A brief description of the principles governing the generation of magnetic resonance imaging, and a review of the most common imaging sequences, including the ultra-fast modalities are presented. The magnetic resonance phenomenon can be described by both classical and quantum mechanical approaches. In this paper, the classical approach is used for the sake of simplicity, although NMR can be more accurately treated by quantum mechanics.

2. Elementary resonance theory

Nuclei of atoms exhibit a proportionality between their total magnetic moment μ and total angular momentum J. These two parallel vectors are related by

$$\mu = \gamma J \tag{1}$$

where γ is the *gyromagnetic ratio* of the nucleus, which is a constant, characteristic of a given nucleus. Note that the value of γ is nucleus-dependent. The γ values of some diagnostically relevant nuclei are listed in Table I.

TABLE I. Properties of some *NMR*-active nuclei.

Nucleus	Spin	*Relative* sensitivity	Gyromagnetic ratio $\frac{\gamma}{2}$ [MHz/T]
^{1}H	$\frac{1}{2}$	1.000	42.58
^{13}C	$\frac{1}{2}$	0.016	10.71
^{19}F	$\frac{1}{2}$	0.870	40.05
^{31}P	$\frac{1}{2}$	0.093	11.26

Regarding the spin *I*, as a quantum operator, then *J* can be defined by

$$J = \frac{hI}{2\pi} \tag{2}$$

where *h* is Planck's constant. The quantum number *m* of I_z (its measurable component) can only take on integer or half-integer values in intervals of 1 from -*I* to *I*, so it follows that the allowed values of M_z are:

$$\frac{-\gamma hI}{2\pi}, \frac{-\gamma h(I-1)}{2\pi}, \cdots, \frac{\gamma h(I-1)}{2\pi}, \frac{\gamma hI}{2\pi} \tag{3}$$

where *I* is the nuclear spin number. The quantity *I* characterises the nuclei. In particular, the proton, the electron and the neutron all have *I* =1/2. Consider a nucleus within a constant magnetic field $B_\circ$ applied parallel to the *Z*-axis. The interaction energy of the nucleus is described by a very simple Hamiltonian:

$$H_z = \frac{\gamma B_0 h I_z}{2\pi} \tag{4}$$

This operator is called the Zeeman Hamiltonian. Since H_z and I_z are proportional to each other, then they have the same eigenfunctions. The eigenvalues of H_z are:

$$E(m) = \frac{\gamma B_0 h m}{2\pi} \tag{5}$$

which are the allowed values of energy for a free nucleus with spin quantum number *I*, and gyromagnetic ratio γ, in the magnetic field $B_\circ$. There are 2*I*+1 such Zeeman levels. The Zeeman energy is also called the energy of spin interaction with the magnetic field. The energy levels are equally spaced because the consecutive values of *m* differ by 1. The energy difference between neighboring levels is;

$$\Delta E = \frac{\gamma B_0 h}{2\pi} \tag{6}$$

Transitions between adjacent energy levels (see Fig. 1), can be induced by applying an alternating magnetic field *B*'= $B_1 \cos(\omega t)$. The energy of photons of this frequency is

$$E = \frac{\omega h}{2\pi} \tag{7}$$

so that the resonance occurs when:

$$\omega = \omega_0 = \gamma B_0 \tag{8}$$

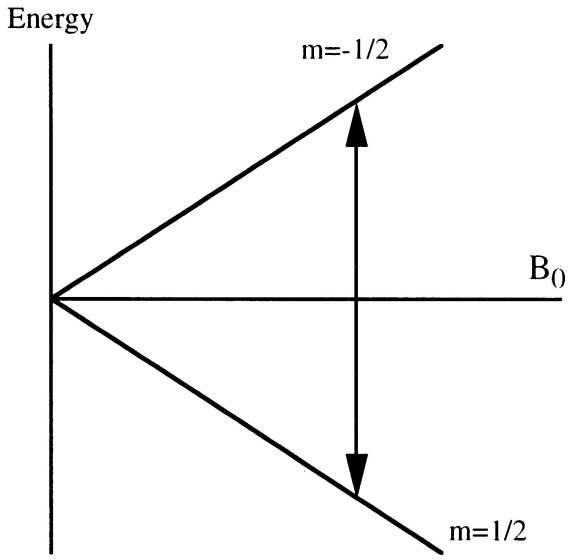

FIGURE 1. The allowed energy levels of a spin 1/2 in a magnetic field.

The spin population difference in the two spin states is related to the energy difference. According to the well-known Boltzmann relationship,

$$\frac{n_2}{n_1} = \exp\left(\frac{\Delta E}{\kappa T}\right) \tag{9}$$

In practice,

$$\Delta E \ll \frac{\Delta E}{\kappa T} \tag{10}$$

Consequently, by first-order approximation

$$\exp\left(\frac{\Delta E}{kT}\right) \approx 1 + \frac{\gamma B_0 h}{2\pi\kappa T} \tag{11}$$

therefore

$$\frac{n_2}{n_1} = 1 + \frac{\gamma B_0 h}{2\pi\kappa T} \tag{12}$$

and for a spin 1/2 nucleus the expression for the fractional population difference is

$$\frac{n_2 - n_1}{n} = tanh\left(\frac{\gamma B_0 h}{2\pi\kappa T}\right) \tag{13}$$

where n=n_1+n_2 is the total number of nuclei, κ is Boltzmann's constant, and *T* is the absolute temperature, and n_1, n_2 are the populations of the two Zeeman levels which obey the Boltzmann distribution. $M_\circ$(bulk magnetization) is proportional to n_1-n_2. In thermal equilibrium there is a net population difference between the energy states. The small size of $\gamma h/2\pi$ $B_\circ$ means that $M_\circ$ is small and consequently the *NMR* sensitivity is very low at room temperature, even at high magnetic fields, such as 1 Tesla. We have an equalization (all components have the same phase at the start of the process)

of the spin populations for a 90° pulse and a population inversion for a 180° pulse. Although it is very small, the population difference between the two spin states generates an observable macroscopic magnetization vector *M* from a spin system. Such spin system is said to be magnetized.

The magnitude of the bulk magnetization vector points exactly along the positive direction of the *Z*-axis at equilibrium and is:

$$M_z^0 = |M| = \frac{\gamma^2 B_0 h^2 n}{4\pi^2 kT} \tag{14}$$

From this, it can be said that magnetization is directly proportional to the external field strength $B_\circ$ and *n*. MRI experiments are often performed with the object being at room temperature, one is limited to increasing the magnitude of the applied field for an increase in the bulk magnetization. Eq. (13) is only valid for a spin-1/2 system, so for a general spin-*I* system, magnetization becomes

$$M_z^0 = \frac{\gamma^2 B_0 h^2 n I(I+1)}{12\pi^2 kT} \tag{15}$$

From Eq. (14) it can be appreciated that magnetic resonance imaging is a low-sensitivity technique since for a magnetic field strength of 1 Tesla and using protons as the source, three in a million protons in an object can be activated to generate the *MR* signal.

3. Larmor precession

We shall study the magnetic moment of a number of nuclei contained in a sample, in which two external fields are applied: a strong constant field applied along the *Z*-axis and an orthogonal Radio Frequency (RF) field. We assume that the external fields, mentioned above, provide the only forces changing the orientation of each nucleus, and that they are uniform throughout the sample. The resultant nuclear moment per unit volume is denoted by μ. We are essentially interested in the variation with time of this vector. The equations describing the Larmor precession of the magnetization can be derived using a classical argument. Classical electromagnetism assures that Eq. (1) holds. A magnetic moment μ in a magnetic field *B*, is subject to a torque *T*:

$$T = \mu \times B \tag{16}$$

If we apply the theorem of preservation of angular momentum to Eq. (16), then *T* becomes

$$T = \frac{dJ}{dt} \tag{17}$$

In the presence of a magnetic field $B=B_\circ k$ we find that by combining Eqs. (1) & (16), the variation of the polarisation vector *M* is given by

$$\frac{dM}{dT} = \gamma\mu \times B_0 k \tag{18}$$

In a frame rotating at angular frequency, ω_e, about the *Z* axis this may be written as

$$\frac{dM}{dT} = \gamma\mu \times (B_0\gamma - \omega_e)\, k \tag{19}$$

In a standard *NMR* experiment, a small oscillating RF field is applied perpendicular to the static field $B_\circ$. In the laboratory frame this can be described by

$$B_x = 2B_1 \cos(\omega t) \tag{20}$$

This may be split into two components rotating at frequencies ω and -ω about the *Z*-axis. To eliminate the time dependence, we use a coordinate system that rotates around the *Z*-axis at a frequency ω transforming this rotating frame, and assuming γ positive, we obtain the following effective field B_{eff}

$$B_{eff} = \left(B_0 - \frac{\omega}{\gamma}\right) k + B_1 i \tag{21}$$

We have neglected the component rotating at -ω. Precession takes place around this rotating field (see Fig. 2), therefore, we can use Eq. (17) and replace $B_\circ$ by B_{eff}.

If ω satisfies the resonance condition

$$\omega = \gamma B_0 \tag{22}$$

B_{eff}=$B_1$and the precession of *M* takes place around the vector B_1. We are referring to precession as seen in the rotating frame of reference in which B_1 is static as indicated in Fig. 3. If we apply the oscillating magnetic field for a short period, $t_1$with amplitude B_1, the magnetization will precess through an angle $\theta=\gamma B_1 t_1$. If $\theta=\pi$, then the pulse inverts the magnetization. This pulse is called a 180° pulse. And, if $\theta=\pi/2$ (90° pulse), then the magnetization is rotated from the *Z*-direction to the -*Y*-direction. After a 90° pulse the magnetization precesses in the laboratory frame, pointing normal to the static field. The pulses described here are usually referred to as *RF pulses*.

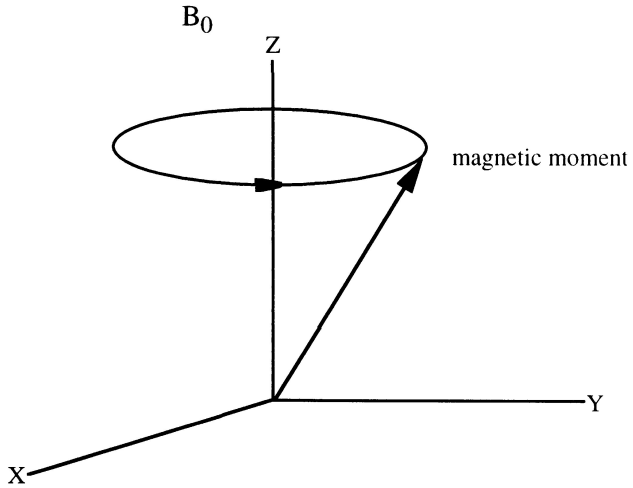

FIGURE 2. The Larmor precession of a magnetic moment in a uniform magnetic field.

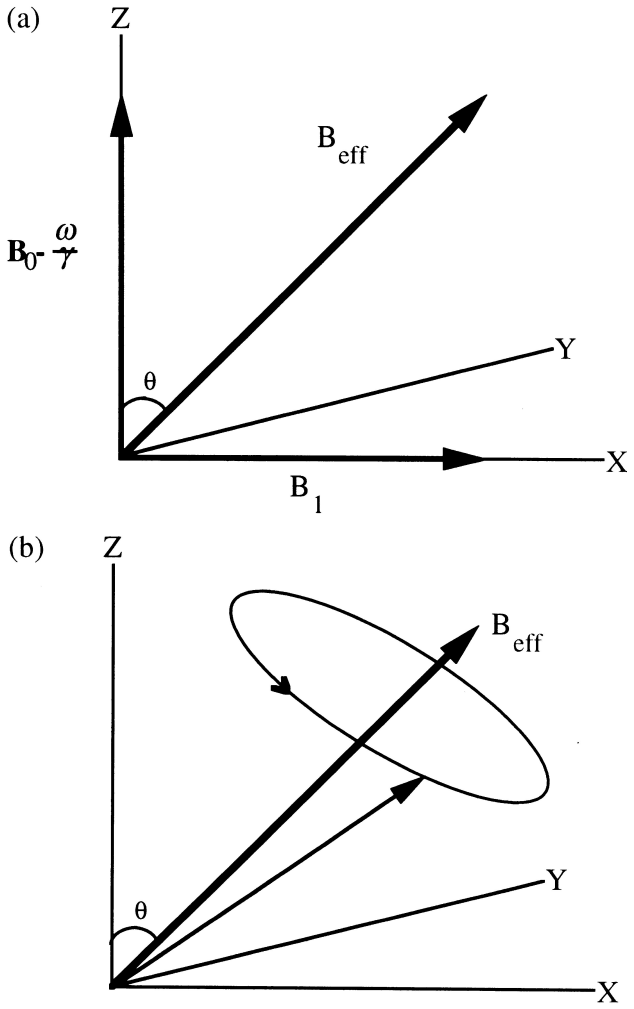

FIGURE 3. a) Effective field B_{eff} in the rotating frame. b) The magnetisation about B_{eff}.

4. The Bloch equations and relaxation times

So far, we have not taken into account the interactions between the spins and their environment, since we were dealing with isolated spins. However, for a sample made up of matter, it is necessary to consider the internal magnetic and electric fields. These fields can cause additional motion of the magnetization, known as relaxation. The problem of the evolution of the magnetization under the influence of the sum of a constant, and a rotating field with simultaneous relaxation was first solved by Bloch [3]. He proposed a set of equations which describe how a spin system evolves. Thus,

$$\frac{dM_z}{dt} = \frac{M_0 - M_x}{T_1} + \gamma \left(M \times B\right)_z \tag{23}$$

$$\frac{dM_x}{dt} = \gamma \left(M \times B\right)_x - \frac{M_x}{T_2} \tag{24}$$

$$\frac{dM_y}{dt} = \gamma \left(M \times B\right)_y - \frac{M_y}{T_2} \tag{25}$$

where B=$B_\circ$+B_1. Two different times T_1 and T_2 have been introduced, which are the longitudinal relaxation time and the transverse relaxation time respectively. The transverse rate of decay may differ from the longitudinal one.

TABLE II. Representative values of approximate relaxation times for hydrogen components of different human tissues at 1.5 Tesla and 37°C.

Tissue	T_1 (ms)	T_2 (ms)
gray matter	950	100
white matter	600	80
muscle	900	50
cerebrospinal fluid (CSF)	4500	2200
fat	250	60
blood	1200	100-200

In terms of the original variables, the complete set of solutions is therefore

$$M_x(t) = \exp\left(\frac{-t}{T_2}\right)\left(M_x(0)\cos(\omega_0 t) + M_y(0)\sin(\omega_0 t)\right) \tag{26}$$

$$M_y(t) = \exp\left(\frac{-t}{T_2}\right)\left(M_y(0)\cos(\omega_0 t) - M_x(0)\sin(\omega_0 t)\right) \tag{27}$$

$$M_z = M_z(0)\exp\left(\frac{-t}{T_1}\right) + M_z(0)\left(1 - \exp\left(\frac{-t}{T_1}\right)\right) \tag{28}$$

Spin-lattice relaxation, which is characterized by T_1, the spin-lattice relaxation time occurs as a result of an exchange of energy between the spin system and the lattice. The lattice is defined as the assembly of sample molecules treated as a reservoir of thermal energy, determined by the motion of molecules. The transverse magnetization is not related to the energy of the spins and its evolution is influenced by quantum transitions, which cause the transfer of energy between spins, leaving the total energy unchanged. This process is called spin-spin relaxation and is defined by T_2, the spin-spin relaxation time.

Inhomogeneity in $B_\circ$ also gives rise to decay of transverse magnetization characterized by a decay time, T_2*. In this case, the precession vector proceeds at different rates in different sections of the sample. This accelerates the process of transverse relaxation, so that $T_2^* < T_2$.

In the rotating frame, Bloch's equations can be solved for continuous irradiation with a weak RF field, so that, saturation is avoided. This saturation condition means that the decay of the transverse magnetization resulting from a $\pi/2$ is complete before another pulse is applied. In other words, after a $\pi/2$ pulse there is no magnetization along the Z-direction: a new $\pi/2$ pulse transmitted at the time would result in no FID signal, as there would be no longitudinal magnetization to rotate into the transverse plane. In this case, the magnetization precesses around B_{eff} (see Fig. 3). Neglecting the transient term, substituting $M_\circ$=$\chi_\circ B_\circ$, and defining

$\omega_\circ=\gamma\, B_\circ$, then the steady state solutions can be expressed as $M_x=\chi'_\circ H_1$and $M_y=\chi''_\circ H_1$

Dispersion mode.

$$\chi' = \frac{\chi_0}{2} T_2 \omega_0 \frac{(\omega_0-\omega)T_2}{1+(\omega_0-\omega)^2 T_2} \tag{29}$$

Absorption mode.

$$\chi'' = \frac{\chi_0}{2} T_2 \omega_0 \frac{1}{1+(\omega_0-\omega)^2 T_2} \tag{30}$$

$$\chi = \chi' - i\chi'' \tag{31}$$

χ is the complex susceptibility and $\chi_\circ$ is the sample's static susceptibility. Eqs. (30) and (31) describe the *NMR* lineshapes predicted by Bloch's equations as shown in Fig. 4.

5. Free induction decay and spin echoes

If a specimen is left in a high magnetic field for a long enough time, protons in the sample will tend to align themselves along the direction of the external magnetic field. Forming a macroscopic nuclear magnetization of the sample. But, if the magnetization is perturbed away from alignment with the field, using a 90° pulse, precession of the resulting magnetization will occur. There will be a gradual dephasing of this magnetization and consequently a loss of coherence of the precessing magnetization. The dephasing of the transverse magnetization causes a gradual decrease of the signal induced in the RF coil, leading to a decaying *NMR* signal which is called the free induction decay (FID). (That is, decay free of B_1). This represents the total time-varying coherent magnetic field derived from the sum over all precessing proton spin fields, which induce a small EMF in any RF coil properly oriented to detect the corresponding flux changes. It can be used to locate the resonance peak for water, and determine the RF amplitude and duration necessary to produce maximum signal. The theoretical expression for the FID for the complex form of a demodulated signal due to an RF spin flip at t=0 is:

$$s(t) \sim \omega_0 \int d^3 r e^{(-\frac{t}{T_2}(\overrightarrow{r}))} |B|(\overrightarrow{r})\,|M(\overrightarrow{r},0)| \times e^{i(t(\Omega-\omega(\overrightarrow{r}))+\phi_0(\overrightarrow{r})-\theta_B(\overrightarrow{r})} \tag{32}$$

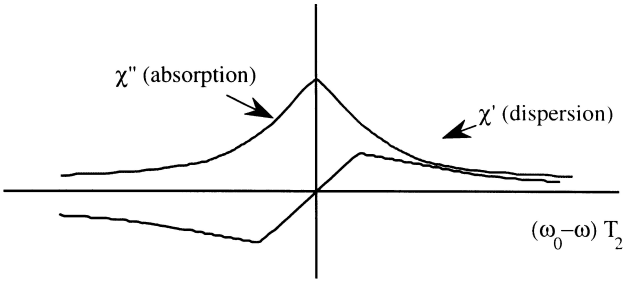

FIGURE 4. Lorentzian lines for absorption and dispersion.

where $\phi_0$is the magnetization phase (the phase angle gives the direction in the X-Y plane of the two-dimensional transverse magnetization vector), Ω is the demodulation reference frequency, and field angle θ_B. In 1950, Hahn [8] showed that an echo of the *MR* signal could be forced by subjecting the sample to two RF pulses. Hahn applied a $\pi/2$ pulse (90° pulse) to a sample to observe a FID which follows a turn-off of the pulse. Inhomogeneities cause a spread in the precession frequency, so that some of the spins go out of phase with respect to the others. Because of this dephasing, the resultant signal decays with a time of the order of $1/(\gamma\Delta B)$, where ΔB is the spread in the static field over the specimen. If however a second $\pi/2$ pulse is applied at a time τ after the first pulse, another signal re-appears at a time 2τ after the initial pulse. He named the signal the *spin echo*. Later, Hahn himself showed the existence of echoes from Bloch's equations. This solution proved that if τ is varied the echo amplitude diminishes exponentially with a time constant T_2. A pictorial description of the process of echo formation in a 90°-τ-90° sequence is shown in Fig. 5.

6. Fourier transform NMR

The early *NMR* experiments used continuous wave (CW) detection. Nowadays, systems use the so called Fourier Transformation *NMR* methods, which employ short intense RF pulses, to excite a wide bandwidth of frequencies simultaneously. Recently the wavelet transform has also been used to generate an image from *MR* signals [9]. The Fourier transform of the resulting FID reveals the mixture of frequencies produced by the applied gradients, chemical shift variations, etc., for on resonance spin species. The FID is the exponential T_2 decay whose Fourier transform is the lineshape of Eq. (30). Experimentally, the lineshape will be broader than that predicted by T_2 relaxation only. This is because the

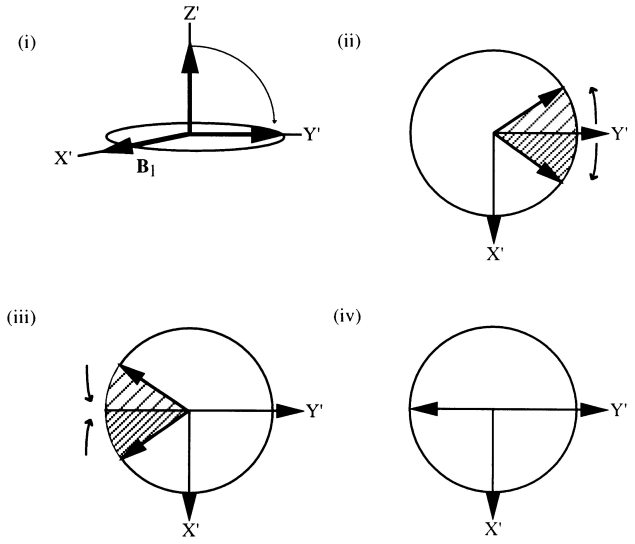

FIGURE 5. The Hahn spin experiment: i) application of $\pi/2$ pulse, ii) dephasing of spins, iii) position of spin isochromats following a π pulse, and iv) position of magnetisation after refocusing.

magnetization is also attenuated by dephasing magnetic field inhomogeneities. This is added to the decay function to yield the effective decay time, where

$$\frac{1}{T_2^*} = \frac{1}{T_2} + \frac{1}{T_{2in}} \tag{33}$$

T_{2in} is the effective relaxation time due only to inhomogeneities. To excite all the spin frequencies of interest the RF pulse should have a bandwidth large enough to span the appropriate frequency range. The bandwidth can be calculated from the Fourier transformation of the pulse shape. The linewidth of the resonance peak can be obtained From Eq. (30). Defining the linewidth Δf as the width at half height, then

$$\Delta f = \frac{1}{\pi T_2} \tag{34}$$

The Fourier transformation of a single FID can produce all the necessary information to create a spectrum.

7. The chemical shift

Other important *NMR* parameters that can distinguish spins in a particular environment are: the self-diffusion coefficient D, the isotropic chemical shift δ, and the hyperfine splitting *J*. In a real spin system, all nuclei in atoms and molecules have associated electrons. If a magnetic field is applied, the surrounding electron clouds tend to circulate in such a direction as to produce a field which opposes that applied, causing a small *chemical shift*. The nucleus experiences a total field:

$$B_{eff} = B_0(1 - d) \tag{35}$$

where *d* is the shielding. This shielding perturbation results in a shift of the resonant frequency for nuclei in different environments, and this resultant effect is very useful in *NMR* spectroscopy. The chemical shift may be expressed as,

$$\delta = \frac{f - f_{TMS}}{f_{TMS}} 10^6 \tag{36}$$

where δ is in parts per million (p.p.m.), f is the resonant frequency of the species of interest, and f_{TMS} is the resonant frequency of a reference substance (*TMS*: tetramethylsilane). The effect of chemical shift is observed in images where more than one chemical is present. The value of δ is very small, usually on the order of a few parts per million and is dependent on the local chemical environmental in which the nucleus is situated. Fat (CH_2) is a well-known example of a chemically-dependent component which is chemically shifted about a 3.35 ppm in Larmor frequency from water (H_20) protons. A large range of δ values exist for biological objects giving rise to many resonant frequencies. It is valid to assume that the resonant frequency range of a spin system can be expresses as

$$|\omega - \omega_0| \leqslant \frac{\omega_{max}}{2} \tag{37}$$

8. Image formation

To form an image is necessary to perform the spatial localization of the MR signals which is normally a two step process. First a slice of the body is selected for imaging. Second a magnetic field gradient can be applied along to any or a combinations of following directions *X*, *Y*, and *Z*, and according to a preestablished imaging sequence to generate an image with a specific orientation.

8.1. Magnetic field gradients

In order to generate an image, it is necessary to measure the spatial variation of MR parameters such as spin density, or the spin-lattice relaxation time, T_1. These variables are not independent of the spatial coordinates of the spin system. These measurements are made by degrading the uniformity of the static magnetic field so that the magnetization precesses at different frequencies. Therefore, there is a variation of resonance frequency across the sample. We may modify the uniformity of the field $B_\circ$ by applying linear magnetic field gradients across the sample. The Hamiltonian describes the interaction of isolated spins at position *r* in a magnetic field gradient as follows

$$H = \frac{h}{2\pi}(\omega_0 I_z + \gamma I \cdot G \cdot r) \tag{38}$$

where *G* is a magnetic field gradient tensor containing nine components. The only terms which contribute significantly are the *Z*-axis ones. Therefore, the effective gradient Hamiltonian is

$$H_1 = \gamma \sum_i (G \cdot r_i) I_{zi} \tag{39}$$

where *G* has the components

$$G_x = \frac{\partial B_z}{\partial x} \tag{40}$$

$$G_y = \frac{\partial B_z}{\partial x} \tag{41}$$

$$G_z = \frac{\partial B_z}{\partial z} \tag{42}$$

To generate a one dimensional image we simply acquire the *NMR* signal in the presence of a spatially varying magnetic field which is added to the uniform field [6-7]. If a linear gradient in the *Z*-direction is employed, the resulting magnetic field parallel to the uniform field is

$$B_z = B_0 + z\frac{\partial B_z}{\partial x} \tag{43}$$

Therefore, the variation of the resonance frequency with position can be expressed

$$\omega_0(z) = \gamma B_z = \gamma(B_0 + G_z z) \tag{44}$$

From Eq. (44) we can appreciate that the gradient gives a linear variation of frequency with position. The magnetic field now has varying amplitude for spins along the *X*-direction. For a one dimensional object, the FID is the sum of all the individual contributions from spins at different positions. The decomposition of the FID into a frequency spectrum is obtained using the Fourier transformation of the *MR* signal. The effect of a linear gradient applied across a two-dimensional sample is shown in Fig. 6.

8.2. Selective excitation

When applying common NMR techniques, the excitation spectra of the applied RF pulses (non-selective or hard pulse) are many times broader than the spin absorption spectrum, so that the whole sample is excited by the RF pulse. In MRI, however, we are usually interested in exciting a thin slice of the sample. This can be done by simultaneously applying a magnetic field gradient and a selective pulse [10]. A suitable shaped selective RF pulse (amplitude modulation in time) is required to excite only a limited section of the frequency spectrum. In the presence of a magnetic field gradient such a pulse will only excite a slice of the sample. The thickness of the slice is proportional to the spectrum width. This effect can be seen from the spatial variation of the transverse magnetization after application of a rectangular pulse of duration t_h in the presence of a *Z*-gradient, G_z. The magnitude of the transverse magnetization is [10]

$$[M_x^2 + M_y^2]^{1/2} = m\,\sin(\theta)[\cos^2(\theta) \times(1-\cos^2(\gamma B_{eff}t_h))^2 + \sin(\gamma B_{eff}t_h)^2]^{1/2} \quad (45)$$

and its phase is defined by

$$\phi = \tan^{-1}\left[\frac{M_x}{M_y}\right] = \tan^{-1}\left[\frac{\cos(\theta)(1-\cos(\gamma B_{eff}t_h))}{\sin(\gamma B_{eff}t_h)}\right] \quad (46)$$

where B_{eff} is the effective field, and θ is the angle B_{eff} makes with *Z*-axis which are given by

$$B_{eff} = \left[B_1^2 + G_z(z-z_0)^2\right]^{1/2} \quad (47)$$

$$\theta = \tan^{-1}\left[\frac{B_1}{G_z(z-z_0)}\right] \quad (48)$$

For small values of B_1 such that

$$\frac{B_1}{G_z(z-z)_0} \ll 1 \quad (49)$$

this reduces to

$$\mid M \mid = \frac{2B_1M_0}{G_z(z-z_0)}\sin\left[\frac{\gamma G_z(z-z_0)t_h}{2}\right] \quad (50)$$

$$\theta = \frac{\gamma G_z(z-z_0)t_h}{2} \quad (51)$$

Thus the shape of the slice (sinc) corresponds to the Fourier transform of the applied pulse (top hat), and the width of the selected slice is inversely proportional to G_z. The phase variation with *Z* means that there will be little total transverse magnetization at the end of the pulse application. The phase variation can, however, be eliminated by applying a gradient, G_z of opposite polarity for a time, $t_h/2$. For general pulse shapes the form of the excited slice follows the pulse spectrum only for low angles, and more powerful techniques must be used to design pulses to excite rectangular slices with large flip angles. The relation between the slice select gradient used and the orientation of the slice plane produced is summarized in Table III.

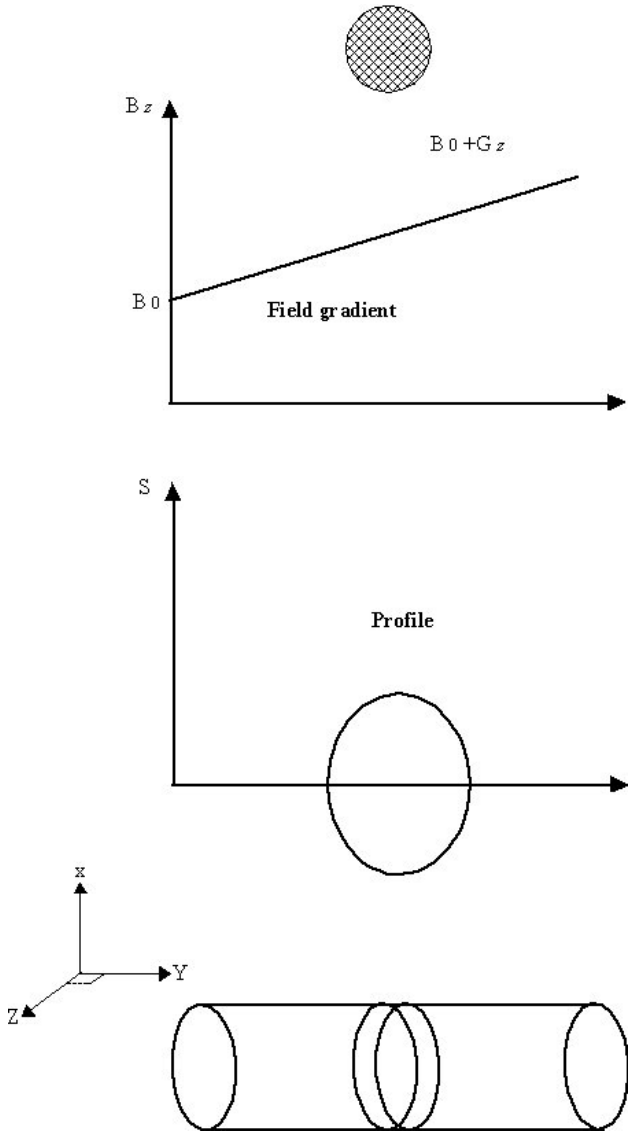

FIGURE 6. a) Application of a linear gradient field to a sample, b) projection of the sample spin distribution, and c) selective excitation of a plane of spins in a cylindrical sample.

TABLE III. Image orientation and the gradient coils used.

Applied slice select gradient	name	slice plane orientation
G_x	sagittal	parallel to *y-z* plane
G_y	coronal	parallel to *x-z* plane
G_z	transverse	parallel to *x-y* plane

Multi-dimensional RF pulses can also be applied in a wide variety of *MR* applications in which transverse magnetization is to be excited, or to be refocused within a well-defined spectral or/and spatial region.

8.3. The *k*-space concept

This is a very important concept in MRI since it allows us to manipulate how the data are acquired, manipulated, and reconstructed for viewing. The *k*-space can be simply defined as the abstract platform onto which data are acquired, positioned, and then transformed into the desired image. There is no such agent in any other imaging modality (x ray-imaging, Positron Emission Tomography, Computerised Tomography, Ultrasound). The choice of the letter *k* is based on the tradition among physicists and mathematicians to use that letter to stand for spatial frequency in other similar equations, and has no particular significance at all.

The *MR* signal as a function of time produced by the slice, omitting relaxation effects [10], is given by

$$S(t) = \int \rho(r) \exp(i\gamma \int_0^t r \cdot G(t')dt')dr \qquad (52)$$

where $\rho(r)$ is the spin density at position *r*. Mansfield and Grannell [7] realized that there is a similarity between the MRI signal and the Fraunhofer diffraction pattern of scattering plane waves. A diffraction pattern is generated and its Fourier transform is the image of the object. In our situation, the plane wave is more of a theoretical concept rather than a real wave, but it can help in the study and design of pulse sequences. Mansfield and Grannell introduced the concept of the reciprocal space wave vector

$$k = \gamma \int_0^t r \cdot G(t')dt' \qquad (53)$$

where *k* is a vector in *k*-space. From Eq. (52) and Eq. (53) the signal can be written as:

$$S(k) = \int \rho(r) \exp(ik \cdot r)dr \qquad (54)$$

It is not very difficult to see that the parameter *k* describes a trajectory scanning through *k*-space as the time *t* of Eq. (54) changes. *k*-space contains all the information required to form an image and allows us to depict graphically most of the MRI techniques. Some *k*-space trajectories of common imaging techniques are shown in Fig. 7. The spatial resolution achievable in MRI is established by the wavelength $\lambda = 2\pi\,|k| - 1$. This parameter indicates that spatial resolution does not depend on the wavelength of the RF at the operating frequency. The resolution of an image in the *X*-direction, can be measured as a function of the maximum spatial frequency k_{max} sampled in the experiment:

$$\Delta x = \frac{\pi}{k_{max}} \qquad (55)$$

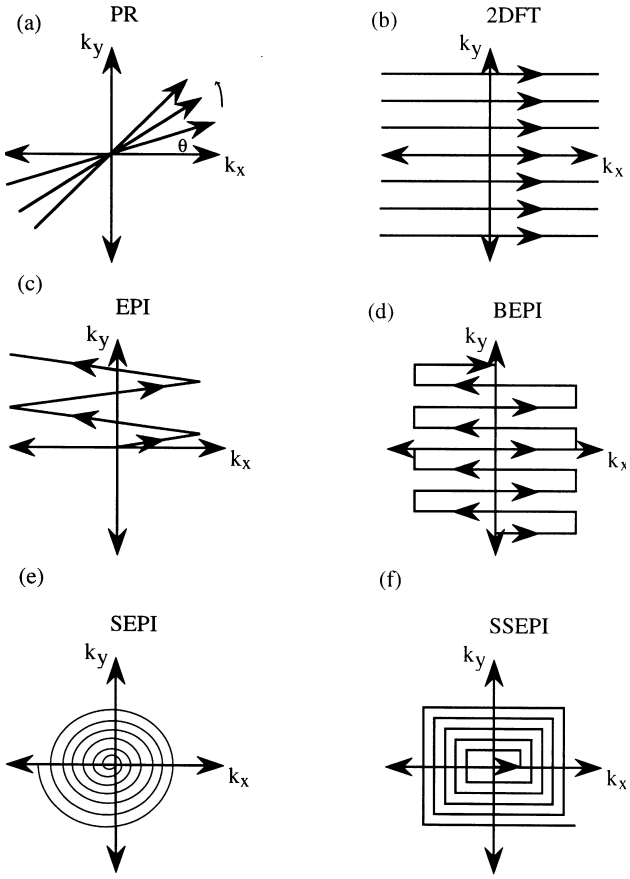

FIGURE 7. *k*-space trajectories corresponding to well-known imaging schemes: a) Projection Reconstruction (PR), b) Two-Dimensional Fourier Transform (2D-FT), c) Echo-Planar Imaging (EPI). d) The Modulus Blipped Echo-Planar Imaging (MBEST). e) Spiral Echo-Planar Imaging (SEPI), e) Square Spiral Echo-Planar Imaging (SSEPI).

For a time independent gradient *G*, which is applied for a time t_d, k_{max} can be written as:

$$k_{max} = \gamma G t_d \qquad (56)$$

Hence, from Eq. (56) the image resolution can be increased by augmenting the gradient amplitude or the time duration, to sample higher spatial frequencies.

9. Magnetic resonance scanner

A number of processes must be completed to produce MR images. These processes include nuclear alignment, RF excitation, spatial encoding, and image formation. In simple terms, an MRI system consists of five major components: a) a magnet, b) gradient systems c) an RF coil system, d) a receiver, and e) a computer system. Fig. 8 shows a block digram of the main components of MR scanner for clinical applications. All of which must be taken into account when designing a suitable site and all of which have their own special problems.

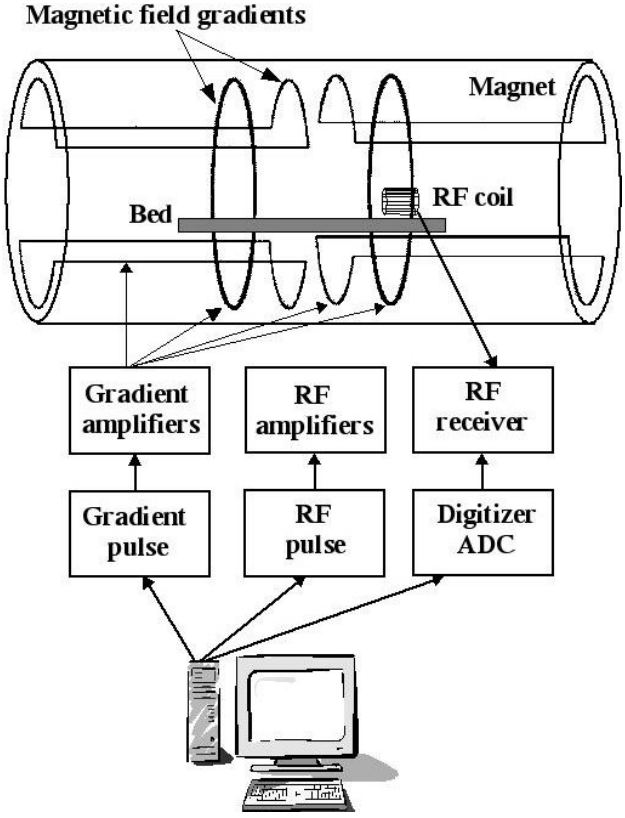

FIGURE 8. Diagram of whole-body magnetic resonance imager.

a) *Magnet*. The magnet aligns the nuclei into low energy (parallel) and high energy (anti parallel) states. Therefore, a strong magnet is necessary to generate a high magnetic field (B_0), which should be uniform over a volume of interest. A high-field magnet provides better *SNR* resolution both in frequency and spatial domains. However, the main requirement for the B_0 field, is that its field uniformity should be very good. A few parts per million over a spherical volume, 50 cm in diameter, are required for a great variety of clinical applications. The optimal field strength and the type of magnet for imaging are dependent on the application so permanent, resistive, or superconducting magnets may be used. For most clinical MRI systems $B_\circ$varies from 0.05 to 3.0 Tesla, and permanent and superconducting magnets are mainly used. Superconducting magnets are made of a niobium-titanium alloy and are cooled to temperatures below 12 K by immersion in liquid helium, whose boiling point is 4.2 K. The main magnet rarely produces a field of sufficient uniformity by itself, so to maintain the magnetic field homogeneity a shim system is necessary.

b) *Gradient coils*. All type of MRI modalities require to deliberately alter the field uniformity by applying a magnetic field gradient $G_z(r)$, which varies linearly with position *r* to spatially encode the NMR signal. Such gradients are generated by passing currents through specially arranged coils of wire, placed on a former that surrounds the imaging subject. Three separate coils are needed in order to produce a linear variation of the Z-component of the magnetic field along each of the three Cartesian directions (see Table III). Many clinical MR systems are capable of producing 40 mT m^{-1} gradients to this end.

c) *RF* coil system. In MRI is necessesary to irradiate the sample under test with an *RF* field (B_1), in order to flip the magnetization away from its equilibrium state and generate a detectable NMR signal. This is usually done with an RF transmitter which is responsible for pulse shape, duration, power, and timing (repetition rate). Since the imaging subject is excited with an RF field, each spin produces a sinusoidal signal at a frequency dependent on the local magnetic field. To detect the signal coming from the spins is necessary a device to couple the nuclei to some external circuitry. These devices are called *RF* coils, or *RF* resonators, or *RF* probes. *RF* coils can be divided in two main groups: volume and surface coils. Volume coils are typically cylindrical-shaped structures, and the most efficient volume coil to the present time is the so called *bird-cage* coil. Surface coils can be subdivided into single-loop coils and array coils (phased- array coils and array of independent coils for ultra-fast imaging schemes).

d) *Receiver* system. To convert the received *RF* signal from the *RF* coil into form suitable for an analog-to-digital converter (ADC) or digitizer, some receiver circuitry is often employed. The signal is first amplified with a low noise amplifier, then is transmitted to a remote location to form an image via a computer processing. The rest of the process involves signal demodulation using a superheterodyne style circuit. This is normally done with respect to the same frequency as the emitted RF radiation.

e) *Computer system*. This system represents the interface through which the user initiates measuring system functions (system test, display images, measure functions) and usually retrieves images. In particular, for the reconstruction process, the computing requirements varies according to the imaging method used, but almost universally some form of Fourier transform (FT) is required. The best algorithm for FT is the fast Fourier transform (FFT), which can be used for two- or three-dimensional images. The computer system should also be able to display images on a high-quality monitor.

10. Overview of MRI methods and techniques

The imaging methods will be divided into four categories: point, line, planar (two dimensions), and three dimensional imaging, depending on the manner in which the image data

points are acquired. This is to say, it is usually by the simple expedient of replacing one stage of the imaging process by a selective excitation. It is clear from their ability to receive the signal, simultaneously from the entire region of interest, that planar and three dimensional techniques will be more efficient than point and line methods, in terms of image signal-to-noise ratio (*SNR*) per unit time, and will therefore be preferred in most situations.

10.1. Point and line methods

The point methods have the advantage of being very simple experimental methods. Usually they do not require a great deal of hardware and the field homogeneity only has to be good over a very small region. One example of these point methods is the so called FONAR (Field Focused Nuclear Magnetic Resonance) method, introduced by Damadian [11]. It is well known, that the FID obtained from a sample located in an inhomogeneous magnetic field will decay rapidly. This occurs because different regions of the sample are located in different magnetic fields. And, the signal therefore has a wide range of frequency components which rapidly dephase giving a shortened FID, and correspondingly a broad lineshape on Fourier transformation. A sample which is sufficiently large to extend beyond the homogeneous region of a magnet will therefore give rise to a signal (to a first approximation) with two components: one which is long-lived from the central homogeneous region, and one which is short-lived from the surrounding non-homogeneous region. A selective pulse with an adequately narrow bandwidth can be used to excite only those spins inside the resonance aperture (signal-producing region). An image can then be produced point by point, by moving the sample relative to the magnet or by relocating the resonance aperture.

Hinshaw [12] introduced another point method which employs three sinusoidal oscillating orthogonal field gradients, which define a small region at their intersection. Only the spins within this region are in a time-invariant magnetic field. This region called the sensitive point, generates a signal which is acquired using a narrow band filter. This is a straight forward technique to implement since there is no need for complicated image reconstruction and little dependence on gradient linearity. This method allows localised *NMR* measurements to be made without the necessity of forming an image, so it could be used to measure T_1. But, the long imaging time is its major disadvantage. These methods are an extension of the point methods. The basic idea is to isolate a line within a three dimensional object and subsequently to distinguish between signal emanating from different points along the selected line. These methods are insensitive to magnetic field inhomogeneities though to a lesser degree than the point techniques.

10.2. Two-dimensional techniques

Most MRI experiments are sequential plane techniques in the sense that a slice of magnetization is excited prior to data acquisition. This is done by using some form of selective irradiation as described previously. Imaging sequences may be divided into two groups: a) frequency encoding of the spin system, and b) phase encoding. We shall start with the simplest technique which uses frequency encoding.

10.2.1. Backprojection reconstruction

This method is normally used in *X*-ray CT, and was introduced into MRI by Lauterbur [6]. The signal obtained from a sample in the presence of an applied gradient corresponds to a one-dimensional projection of the object onto the axis of the gradient. An image can be constructed by altering the direction of this gradient to collect a number of projections of the object, and then processing these profiles using a reconstruction algorithm. The total spin density contributing to a frequency $\Delta\omega = \gamma G\phi r$, to each ray ($r$,$\phi$), is given by the line integral:

$$P(r,\phi) = \int\limits_{\Gamma,\phi} \rho(x,y)ds \qquad (57)$$

where *s* is the distance along the ray direction. Each value of $P(r,\phi)$ is called a *ray sum*, and the set of values for a given gradient orientation ϕ as the projection at angle ϕ. Eq. (57) represents a *NMR* spectrum, which is the Fourier transform of the FID obtained from the gradient G_ϕ. A set of projections $P(r,\phi)$ is acquired by rotating the gradient angle. These are then filtered, and back projected to form an image.

10.2.2. Fourier imaging

The Fourier method was first developed by Kumar and *et. al*, in 1975 [13], and can be considered to be a typical two dimensional spectroscopy technique. The most popular class of planar methods are currently the two dimensional Fourier techniques, for short 2D-FT. The basic idea is to apply a 90° RF pulse, and a slice selection gradient to generate an FID which evolves first under the influence of a field gradient, G_y for a time t_y, followed by a second gradient, G_x with duration *t*, which is applied at a right angles to the first. The signal is phase encoded during the application of the first gradient, and sampled for times t_x during the spatial encoding, read gradient, G_x. Excluding relaxation effects, the signal is:

$$S(t_x,t_y)=\iint \rho(x,y)\exp\left[i\gamma(G_x x t_x+G_y y t_y)\right]dxdy \quad (58)$$

The experiment is then repeated with an incrementing period of evolution under the gradient G_y. In these experiments, *k*-space is filled with one line at a time. After the full data acquisition is done, a two dimensional Fourier transform (2D-FT) yields the spin density distribution. The sequence of *RF* pulses and gradient pulses is shown in Fig. 9. Edelstein and *et al.* [14] modified the Fourier imaging method, to introduce another method called spin-warp imaging, in which a phase variation is generated by changing the gradient amplitude with the phase encoding carried out for a constant time period. This has the advantage that effects remain constant

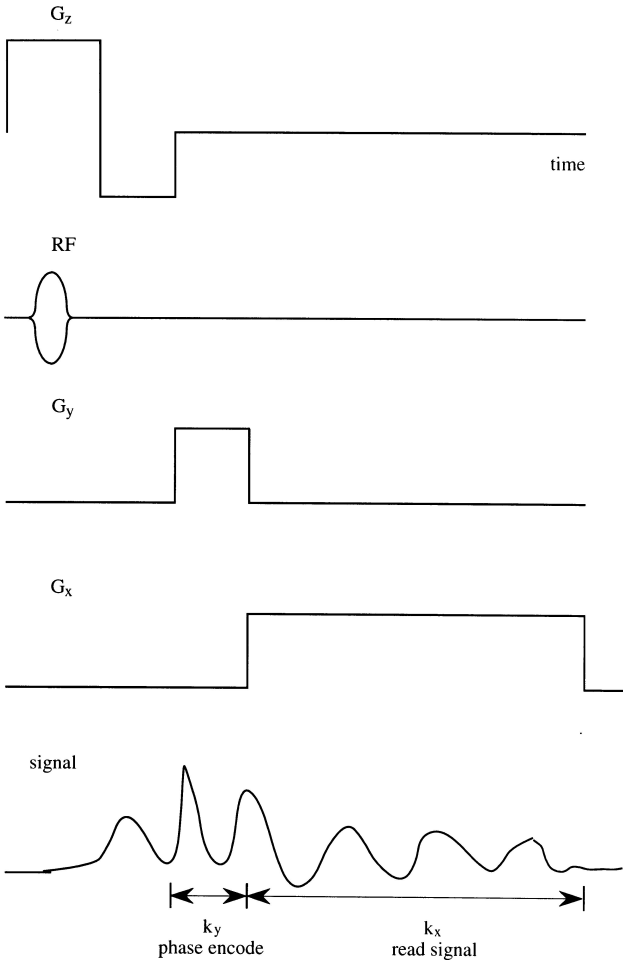

FIGURE 9. The sequence of RF pulses and gradient pulses for 2D-Fourier Transform Imaging.

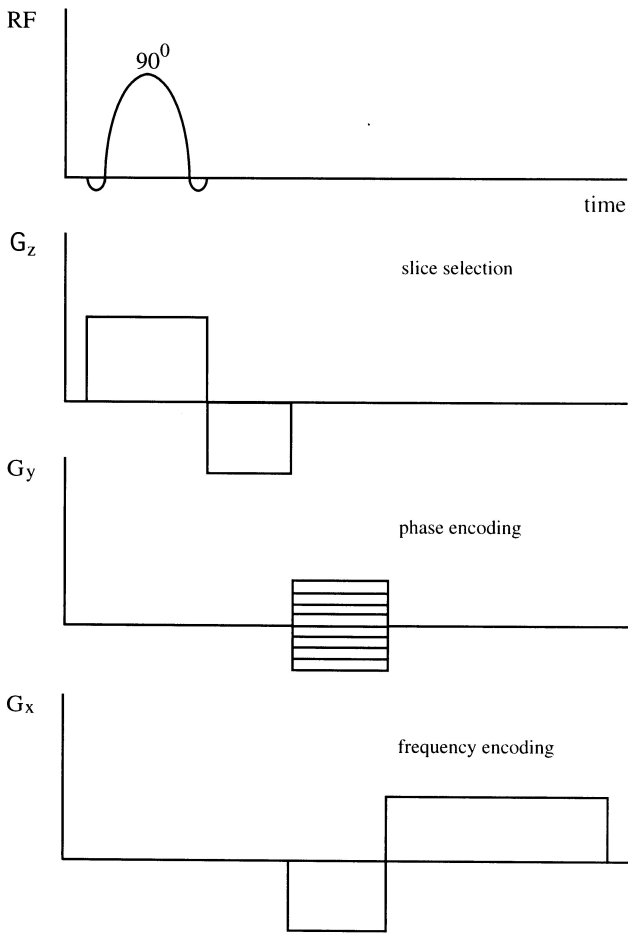

FIGURE 10. A timing diagram for the 2D-FT Spin Warp scheme.

throughout the experiments. A timing diagram for the 2D-FT spin-warp imaging sequence is shown in Fig. 10.

10.3. Full and half Fourier imaging

Whenever the four *k*-space quadrants are scanned, filling the whole of the space, this is designated as a Full Fourier technique. The Fourier transform generates information containing real and imaginary parts with a well defined phase. Taking the modulus of the two parts, gives rise to modulus images in which all phase effects are removed. However, these methods can require long imaging times. To abbreviate the long imaging times of the Full Fourier methods, we can scan only half of the *k*-space [15-16], and then reconstruct the other half using the Hermitian symmetry property of the Fourier transform of the *MR* signal, S(-*k*) = S*(*k*) [15]. Then, in some cases only half the number of the experiments are required. This method requires zero filling of the data before Fourier transformation. Filtering is needed to avoid ringing at the edges produced by the truncating step function. Phase variation causes problems since the Hermitian symmetry is lost. Such phase variation results from field inhomogeneity, misalignment of the signal detection, and gradient eddy currents. These problems can be overcome by using another type of partial sampling scheme, which makes use of slightly more than half of the *k*-space data in one encoding direction [17-18]. This enables us to construct a coarse phase map from the symmetric data around the origin, which will be employed afterwards to correct the phase errors, see Fig. 11(e). Some Half Fourier sampling strategies are illustrated in Fig. 11.

10.4. Three-dimensional techniques

It is possible to extend the two dimensional techniques to produce three dimensional imaging. Three-dimensional data sets can be generated in many different ways from Fourier techniques, for example, by multislice imaging or by using additional phase encoding. The multislice technique can produce images of different sections. The slice of the object goes through a cycle during the interval *TR*, during this time a different slice is selected and then imaged. Most of the imaging time is spent in waiting for T_1 recovery of magnetization (*TR*). A 3D FT image can be acquired by repeating a 2D-FT process a certain number of times without slice selection, where the repetition number depends on the number of slices that are required. The information in the *Z*-axis is encoded

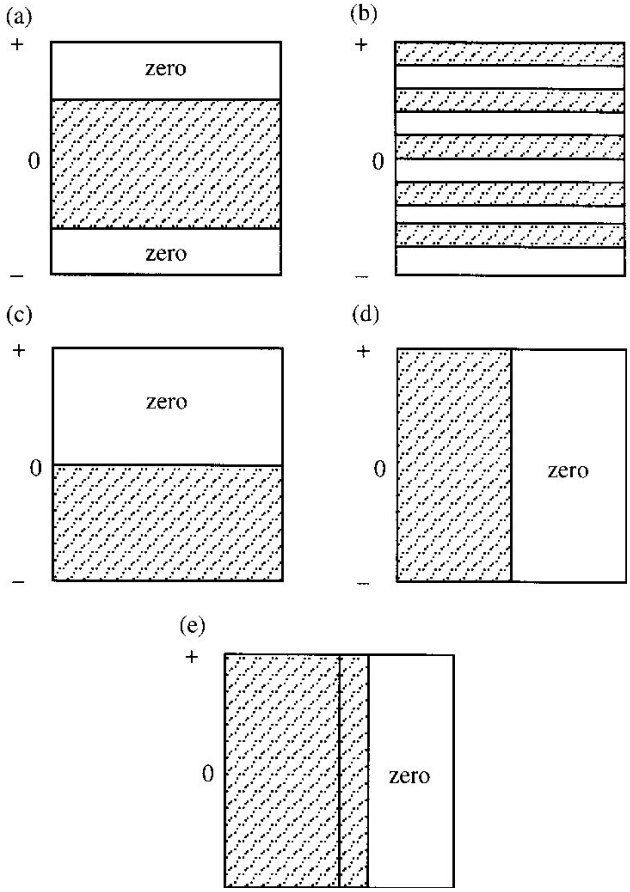

FIGURE 11. *k*-space can be scanned in different ways: a) symmetrically about the centre, b) alternate phase-encoding lines, c) non-positive phase-encoding steps, d) in the readout direction, and e) partial scanning in the readout direction. The horizontal direction is the readout time. The shaded areas correspond to the experimentally acquired data and the other lines are zero.

in the same way as it is encoded along the *Y*-axis by the use of an additional phase encoding gradient. The Fourier transform is applied successively three times to reconstruct the 3D image.

10.5. Chemical shift imaging

MRI and MRS have been developed somewhat independently, and the information provided by these two techniques is complimentary. MRI exclusively uses the proton (^{1}H) resonance, to yield spatially-resolved images with no discrimination among signals arising from hydrogen nuclei existing in different chemical groups (no chemical shift resolution). MRS is able to yield NMR spectra in which chemical shift resolution is very important. Such spectra contains no spatial information. Thus it has long been desired to obtain both spectrally and spatially-resolved information in a single study. These two sources of biological information can be put together in the so called chemical shift imaging or spectroscopic imaging. This imaging technique is referred to the process of selectively imaging (or obtaining the spatial distribution) of identical nuclei that different levels of magnetic shielding due to their chemical environments as shown in Eqs. (35) & (36). The possibility of observing body chemistry at the same time as producing an image is a bonus which, if applied clinically, could uniquely pinpoint regional metabolic disorders in tissues and organs.Via chemical shift imaging, the clinician and the researcher are able to glean information of a truly chemical and biochemical nature in a completely non-invasive manner.

11. Contrast and signal-to-noise ratio (SNR)

An important aim of imaging for diagnostic purposes is to be able to distinguish between diseased and neighbouring normal tissue. MRI offers important advantages when compared with other imaging modalities due to its excellent soft tissue discrimination of the images. MRI has an abundance of signal-manipulating mechanisms, as the signal is dependent of a wide variety of tissue parameters. A contrast in the image can then be created to meet certain demands. Image contrast is defined in terms of differences in image intensity as follows:

$$C_{AB} = \frac{|Im_A - Im_B|}{Im_{ref}} \tag{59}$$

where $Im_{\mathcal{A}}$ and Im_B are the image intensity of tissues *A* and *B*, and Im_{ref} is a normalising value. *Im* is a function of spin density σ, T_1, T_2,T_2^* and diffusion coefficients *D*. If the data acquisition parameters are chosen such that the T_1 effect is dominant, then

$$C_{AB} \approx f(T_1) \tag{60}$$

and the resulting images is said to carry T_1 contrast or a T_1 weighting. Similarly for T_2 contrast and spin density contrast:

$$C_{AB} \approx f(T_2) \tag{61}$$

and

$$C_{AB} \approx f(\sigma) \tag{62}$$

Spin density contrast is linearly proportional to the tissue spin density difference, whereas T_1, T_2 contrasts have an exponential dependence on the tissue T_1, T_2 values. Normal soft tissue usually have a small variation in spin density, but have quite different T_1 values. Therefore, T_1-weighted imaging is an effective method to obtain images of a good anatomical definition. Many disease states are characterized by a change of the tissue T_2 value, and T_2-weighted imaging is a sensitive method for a disease detection. Fig. 12 shows T_1 -weighted and T_2-weighted images of brain obtained at 1.5 Tesla.

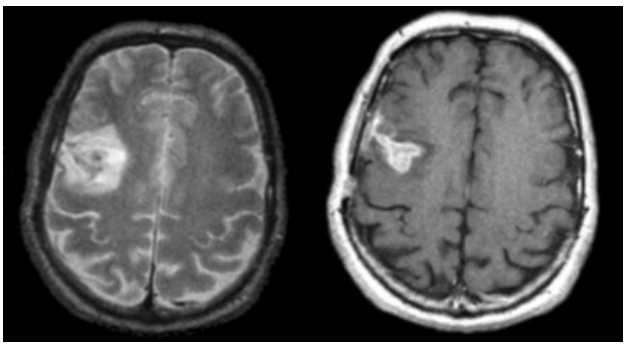

FIGURE 12. A T_2-wheighted image (left) and T_1-weighted image (right) of the human brain.

In any physical measurement there is always present noise either random or systematic which diminish the image quality. Random noise often arises in an imaging system because of spontaneous fluctuations such as the thermal noise (Brownian motion) of free electrons inside real o equivalent electrical components. This noise is sometimes called Johnson noise. The degree to which noise affects a measurement is generally characterized by the *SNR*. This is the ratio of the amplitude of the signal received to the average amplitude of the noise. The signal is the voltage induced in the receiver coil by the precession of the magnetization in the transverse plane. The noise is generated by the presence of the patient in the magnet, and the background electrical noise of the system (coil and electronics). It is also known that the variance of the fluctuating noise voltage is

$$\sigma_{thermal} = \sqrt{4\kappa TR\, BW} \tag{63}$$

where *R* is the effective resistance of the coil loaded by the body, and *BW* is the bandwidth of the noise-voltage detecting system. Both the signal and noise are detected by the receive coil, and the bandwidth is determined by the cutoff frequency of the analog low pass filter. The *SNR* can be defined as,

$$SNR = \frac{\text{signal}}{\text{resistance}} = \frac{S(k)}{R_{eff}} \tag{64}$$

$$SNR = \frac{\int \rho(r)\exp(ik\cdot r)dr}{R_{\text{body}} + R_{\text{coil}} + R_{\text{electronics}}} \tag{65}$$

From Eq. (65) can be appreciated that to increase the *SNR* can be done by a) reducing the effective resistance: this can be achieved by reducing the coil and electronics resistance, this demands better coil designs with low resistance values, b) increasing the *MR* signal with high-field *MR* scanners. High field *MRI* promises to improve anatomic imaging quality by factors, and to bring metabolic and functional imaging to the forefront of diagnostics modalities. There are systems available with field strengths up to 22 Tesla, but for clinical purposes the highest field is 3 Tesla. Although it is possible to purchase whole-body systems of 7 T or 8 T for MRI applications in humans. The *SNR* is also an important parameter to measure performance of a *MR* imager.

The size of the spatial features that can be distinguished in a MR image can be defined as the resolution, and does not depend on the wavelengths of the input *RF* field.

12. Ultra-fast imaging

The development of faster magnetic resonance imaging has mainly been motivated by the long acquisition times compared to physiological motion and patient tolerance. These long times cause imaging artefacts, a limited number of applications and increased costs. Respiration, pulsation peristalsis occur during the exam can result in substantial distortion of the image. Artefacts from patient motion can drastically degrade the image quality, due to discomfort originated by exams with long duration times. This exacerbated in patients with pain and suffering from claustrophobia. Shorted scanning times can reduce the cost of a conventional MRI exam.

MRI offers alternatives to reduced-time acquisition schemes. In the most commonly used imaging sequence, multislice two-dimensional Fourier transform (2D-FT), the scan time T_{scan} is given by the following simple relationship:

$$T_{scan} = N_Y\ TR\ NEX \tag{66}$$

where *N* is the number of phase-encoding samples, *TR* the pulse repetition time, and *NEX* the number of excitations (also termed number of acquisitions or number of averages) used for signal averaging.

12.1. Fast Fourier imaging

The spin-warp imaging technique owes its popularity in the clinical environment to its robustness, however in its simplest form it requires long imaging times. In an effort to reduce scan time, Haase and co-workers [19] introduced an imaging method called Fast Low Angle Shot: FLASH. This is basically the gradient echo version of the 2D-FT technique with a very short repetition time *TR*. Reduction of the echo time necessitates the use of a low angle RF pulse for slice selection, typically around 15°, for maximum *SNR*. There are other techniques which are based on the same principles, such as the Snapshot/Turbo FLASH and Gradient Recalled Acquisition in the Steady State (GRASS) techniques [20]. GRASS is a very similar technique to FLASH, which only differs in that an additional phase encoding gradient is applied after the sampling period. This gradient has an opposite sign to the first one, so it can rephase any transverse magnetization remaining at the end of the experiment. Consequently, the *SNR* is improved and image artefacts are removed.

12.2. Echo-planar imaging

Echo Planar Imaging (EPI) was introduced by Mansfield in 1977 [21], and is a true snapshot technique which enables the formation of a complete image in 30-100 ms. The rapid nature of this technique is due to the fact that only one RF

excitation is needed per image. It thus allows the acquisition of a two-dimensional image from only one FID. Following the excitation of a slice, the signal is sampled under the influence of two orthogonal gradients. A gradient G_x (*X*-axis) is modulated rapidly to generate a series of gradient echoes. This forms the frequency encoding part of the experiment. In conjunction with G_x, another gradient G_y (*Y*-axis) is applied: this gradient is either blipped or continuous and performs the phase encoding part of the experiment. This combination of gradients serves to encode each point in the image with a different degree of phase evolution between echoes and frequency during an echo. A train of phase encoded echoes is thus acquired. After some data manipulation required because of the effect of evolution of sequential echoes under positive and negative read-out gradient lobes, it is possible to apply a 2D-FT to create an image. Generation of a 128×128 image requires the production of 128 gradient echoes, with each echo being sampled using 128 data points. EPI has undergone many modifications since its introduction in 1976. The original forms of EPI were called Double Echo Planar Imaging (DEPI) and Fast Low Angle Excitation Echo Planar Technique (FLEET) [22]. DEPI is a two shot experiment with G_y having positive and negative starting phase in alternate shots. The data sets are corrected by splicing together all the echoes formed in totally positive and totally negative gradients. Two images are produced, which can be re-registered and added to yield an improvement in *SNR*. Flip angles of $45°$and $90°$ were used to minimize the acquisition time. These techniques originally used a constant phase encoding gradient. Ljunggren [23] first proposed replacing the continuous phase encoding gradient by a blipped gradient: G_y blips are applied in the spaces between echoes. The resulting trajectory through *k*-space is a square raster scan. Correction of the time evolution can be achieved by simply reversing the data which makes up every alternate echo prior to FT. The scan still starts at the *k*-space origin, and zero filling is still required. This single shot technique is called Blipped Echo Planar Imaging (BEPI) or Blipped Echo Planar Single pulse Technique (BEST) [24-25]. BEST is susceptible to the effect of magnetic field inhomogeneities which cause phase errors. Therefore, it is important to ensure that the transverse magnetization is completely in phase at the start of the experiment. This implies the use of a $180°$ pulse which will be applied immediately following slice selection. Data acquisition begins at the point of maximum signal, when the magnetization is completely refocused. The modulus version of this experiment, called MBEST, is found to be essentially identical to BE21ST, except for the addition of a large negative G_y gradient pulse prior to data acquisition. *k*-space is fully scanned and the FT data produces a modulus image which is considerably more robust and less susceptible to phase errors. The MBEST timing diagram is shown in Fig. 13. EPI is a compact technique which is easily adaptable as an imaging module applied after any suitable spin preparation experiment, such as Inversion Recovery [26] and Spin Echo EPI [27].

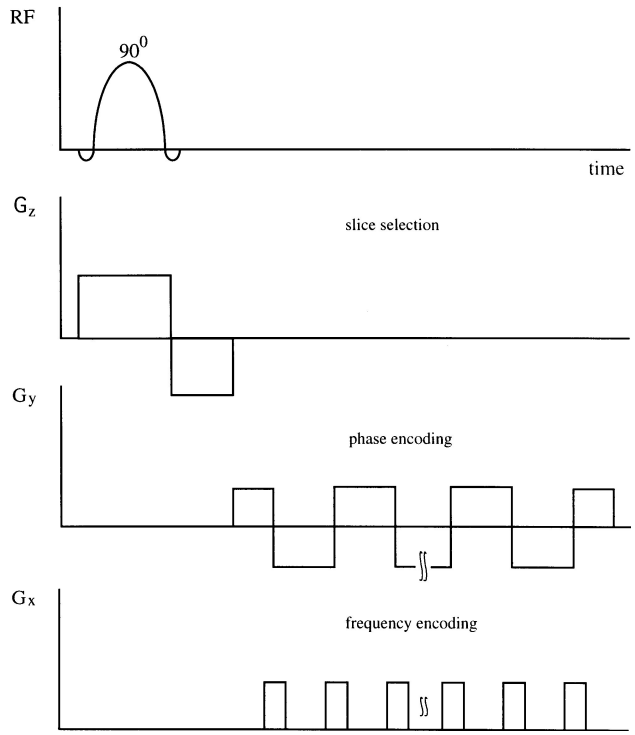

FIGURE 13. A timing diagram for MBEST technique.

Three dimensional EPI techniques can also be obtained as an extension of EPI in two dimensions. In the Echo Volumar Imaging (EVI) technique [28], the signal is sampled under the influence of three gradients: one of them has a constant polarity and the other two are modulated. The trajectory of *k*-space is extended to three dimensions which are covered as in two- dimensional EPI. A time of over 100 ms is needed to complete a scan and form a 3D EPI image. Other examples of 3D EPI are: multislice EPI and Phase Encoded Volumar Imaging (PEVI) [29].

12.3. Parallel imaging: SENSE and SMASH techniques

Reduction of acquisition time without diminishing the SNR is a paramount challenge in MRI. To meet this challenge, two important schemes have been recently introduced: a) Sensitivity encoding for fast MRI (SENSE) [30], and b) Simultaneous Acquisition of Spatial Harmonics (SMASH) [31]. These imaging schemes are based on the difference in sensitivities between individual coil elements in a receive array to reduce the number of gradient encoding steps required for imaging. Since they make use of the individual coil sensitivities, they are called parallel imaging techniques. Each coil in an array receives a signal from a region of interest. By appropriately combining the images from each coil, an overall image of higher sensitivity and/or broader field of view can be obtained than with a single coil element. The individual coil sensitivities are used to reconstruct a full image from a partial *k*-space acquisition. A *g* factor (noise amplification factor) is introduced due to the image reconstruction process.

Parallel imaging is useful for any application where minimum acquisition time is paramount. Applications include real-time imaging, first-pass bolus contrast imaging, cardiac imaging, and EPI. These imaging sequences heavily depend on the coil sensitivity, so the interest to develop new coils for parallel imaging has reborned again. These imaging techniques have a very promising future since are able to generate an image in less than a few milliseconds, reduce motion artefacts, and improve image quality. The *g* factor is a limitant issue when using parallel imaging.

Acknowledgment

I would like to thank Sir Peter Mansfield and Professor Richard Bowtell for illuminating conversations.

1. F. Bloch, W.W. Hansen, and M.E. Packard, *Phys. Rev.* **69** (1946) 127.
2. F. Bloch, *Phys. Rev.* **70** (1946) 460.
3. F. Bloch, W.W. Hansen, and M.E. Packard, *Phys. Rev.* **70** (1946) 474.
4. E.M. Purcell, H.C. Torrey, and R.V. Pound, *Phys. Rev.* **69** (1946) 37.
5. N. Bloembergen, E.M. Purcell, and R.V. Pound, *Phys. Rev.* **73** (1948) 679.
6. P.C. Lauterbur, *Nature* **242** (1973) 190.
7. P. Mansfield, P.K. Grannell, *J. Phys. C* **6** (1973) L422.
8. E.L. Hahn, *Phys. Rev.* **80** (1950) 580.
9. J.B. Weaver, Y. Xu, D.M. Healy, and J.R. Driscoll, *Magen. Reson. Med.* **24** (1992) 275.
10. P. Mansfield, PG. Morris, NMR Imaging in Biomedicine, Supplement 2 in Advances in Magnetic Resonance (Waugh, J.S., Editor), Academic Press, New York, 1982.
11. R. Damadian, M. Goldsmith, L. Minkoff, *Physiol. Chem. Phys.* **10** (1978) 285.
12. W.S. Hinshaw, *Phys. Lett. A* **48** (1974) 87.
13. A. Kumar, D. Welti, R.R. Ernst, *J. Magn. Reson.* **18** (1975) 69.
14. W.A. Edelstein, J.M.S. Hutchinson, G. Johnson, and T. Redpath, *Phys. Med. Biol.* **25** (1980) 751.
15. N.S. Cohen and R.M. Weisskoff, *Magn. Reson. Imaging* **9** (1991) 1.
16. H. Fischer, F. Schmitt, H. Barfuss, H. Bruder, 7th Ann. Meet. Soc. Mag. Res., San Francisco, 1988.
17. C.H. Oh, S.K. Hilal, J.B. Ra, Z.H. Cho, Books of Abstracts, 6th Ann. Meet. Soc. Mag. Res., New York, 1987.
18. L.E. Crooks, M. Arakawa, J.D. Hale, J.C. Hoenninger, J.C. Watts, L. Kaufman, D.A. Feinberg, Books of Abstratcs, 5th Ann. Meet. Soc. Mag. Res., Quebec, 1986.
19. Haase, A., Frahm, J., Matthaei, D., Hanicke, W., Merboldt, K. D., *J. Magn. Reson.* **67** (1986) 258.
20. P.V.D. Meulen, J.P. Groen, and A. M. C. Tinus Brutink, *Magn. Reson. Imag.* **6** (1988) 335.
21. P. Mansfield, *J. Phys. C: Solid State Phys.* **10** (1977) L55.
22. R. Ordidge, Ph D Thesis, University of Nottingham, 1981.
23. S. Ljunggren, *J. Magn. Reson.* **54** (1983) 338.
24. A.M. Howseman *et al.*, *Brit. J. Rad.* **61** (1988) 822.
25. B. Chapman *et al.*, *Magn. Reson. Med.* **5** (1987) 246.
26. M.K. Stehling, R.J. Ordidge, R. Coxon, P. Mansfield, *Magn. Reson. Med.* **13** (1990) 514.
27. I.L. Pykett and R.R. Rzedizan, *Magn. Reson. Med.* **5** (1987) 563.
28. P. Mansfield, R.J. Ordidge, R. Coxon, *J. Phys. E: Sci. Instrum.* **21** (1988) 275.
29. A.M. Blamire, Ph D Thesis, University of Nottingham, 1990.
30. K.P. Pruessman, M. Weiger, M.B. Scheidegger, and P. Boesiger, *Magn. Reson. Med.* **42** (1999) 952.
31. D.K. Sodickson and W.J. Manning, *Magn. Reson. Med.* **38** (1997) 591.
32. A. Abragam, *Principles of Nuclear Magnetism* (Clarendon Press, Oxford, 1989).
33. C.P. Slichter, *Principles of Magnetic Resonance*, 3rd Edition, (Springer-Verlag, Berlin, 1992).
34. D.G. Gadian, *Nuclear Magnetic Resonance and Its Applications to Living Systems.* 2nd Ed., (Oxford, University Press, 1995).
35. P.G. Morris, *Nuclear Magnetic Resonance Imaging in Medicine and Biology* (Clarendon Press, Oxford, 1986).
36. C.N. Chen, D.I. Hoult, *Biomedical Magnetic Resonance Technology* (Adam Hilger, IOP Publishing, Britain, 1989).
37. M.A. Foster, J.M.S. Hutchinson, (Editors), *Practical NMR Imaging*, (IRL Press, Oxford, 1987).
38. E.M. Haacke, R.W. Brown, M.R. Thompson, R. Venkatsen, *Magnetic Resonance Imaging*, Physical Principles and Sequence Design, (Wiley-Liss, New York, 1999).
39. Z.P. Liang, P.C. Lauterbur, *Principles of Magnetic Resonance Imaging*, A signal processing perspective, (IEEE Press, New York, 2000).